Supporting Information：

Highly Selective Electrocatalytic Reduction of CO_2 to Methane on Cu–Bi Nanoalloys

Zhijiang Wang,[*,†,#] Qi Yuan,[⊥] Jingjing Shan,[†] Zhaohua Jiang,[†,#] Ping Xu,[†] Yongfeng Hu,[§] Jigang Zhou,[§] Lina Wu,[‖] Zhuangzhuang Niu,[†] Jianmin Sun,[*,†] Tao Cheng,[*,⊥,‡] William A. Goddard III,[*,‡]

† MIIT Key Laboratory of Critical Materials Technology for New Energy Conversion and Storage and #State Key Laboratory of Urban Water Resource and Environment, School of Chemistry and Chemical Engineering, Harbin Institute of Technology, Harbin 150001, China;

⊥ Institute of Functional Nano & Soft Materials (FUNSOM), Jiangsu Key Laboratory for Carbon Based Functional Materials & Devices, Soochow University, Suzhou, Jiangsu 215123, China;

‖ Department of Radiology, Molecular Imaging Research Center of Harbin Medical University, the Fourth Hospital of Harbin Medical University, Harbin 150001, China;

§ Canadian Light Source Inc., Saskatoon, Saskatchewan S7N 0X4, Canada;

‡ Materials and Process Simulation Center (MSC) and Joint Center for Artificial Photosynthesis (JCAP), California Institute of Technology, Pasadena, California 91125, United States;

*Correspondence to wangzhijiang@hit.edu.cn; sunjm@hit.edu.cn; tcheng@caltech.edu; wag@wag.caltech.edu.

Experimental Procedures

Synthesis of catalysts

Cu nanoparticles: PVP K30 (0.2 mmol, 22.2 mg, BASF) and copper (II) nitrate (0.2 mmol, 37.5 mg, Sigma-Aldrich) were dissolved into 20 ml ethylene glycol (Alfa Aesar) saturated by Ar. 3ml methanol solution of $NaBH_4$ (2 mmol, l75.66 mg, Sigma-Aldrich) was added dropwise to the precursor solution under ice bath condition. Then 20 mg carbon black (Cabot Corporation) was added into the resultant black colloid and sonicated for 30 minutes. Nanoparticles were collected by centrifugation and washed three times with absolute ethanol and dried at ambient temperature for 12 h.

Cu_9Bi_1 nanoparticles: Cu_9Bi_1 nanoparticles were synthesized by a procedure similar to the Cu nanoparticle. But the precursor solution was composed of PVP K30 (0.2 mmol, 22.2 mg, BASF), copper (II) nitrate (0.18 mmol, 33.8 mg, Sigma-Aldrich), bismuth (III) nitrate pentahydrate (0.02 mmol, 9.7 mg) and 20 ml ethylene glycol (Alfa Aesar).

Cu_7Bi_1 nanoparticles: Cu_7Bi_1 nanoparticles were synthesized by a procedure similar to the Cu nanoparticle. But the precursor solution was composed of PVP K30 (0.2 mmol, 22.2 mg, BASF), copper (II) nitrate (0.16 mmol, 30 mg, Sigma-Aldrich), bismuth (III) nitrate pentahydrate (0.04 mmol, 19.4 mg) and 20 ml ethylene glycol (Alfa Aesar).

Cu_3Bi_1 nanoparticles: Cu_3Bi_1 nanoparticles were synthesized by a procedure similar to the Cu nanoparticle. But the precursor solution was composed of PVP K30 (0.2 mmol, 22.2 mg, BASF), copper (II) nitrate (0.1 mmol, 18.8 mg, Sigma-Aldrich), bismuth (III) nitrate pentahydrate (0.1 mmol, 48.5 mg) and 20 ml ethylene glycol (Alfa Aesar).

Bi nanoparticles: Bi nanoparticles were synthesis by a procedure similar to the Cu nanoparticle. But the precursor solution was composed of PVP K30 (0.2 mmol, 22.2 mg, BASF), bismuth (III) nitrate pentahydrate (0.2 mmol, 97 mg) and 20 ml ethylene glycol (Alfa Aesar).

Physical characterizations

The morphologies of the prepared samples were obtained using a transmission electron microscope (TEM) on a Tecnai G2 F30 electron microscope under an accelerating voltage of 300 keV. TEM samples were prepared by dropping a diluted suspension onto amorphous carbon-coated copper grids and drying in the air. An energy-dispersive X-ray spectroscopy (EDS) attached to the TEM machine provided in situ determinations of the composition of the samples. The crystal structures of the synthesized samples were recorded on a Bruker AXS D5000 diffractometer by recording their X-ray diffraction (XRD) patterns. X-ray photoelectron spectroscopy (XPS) of samples was measured using a PHI 5700 X-ray photoelectron spectrometer equipped with a monochromatic Al Kα X-ray source. X-ray absorption

spectroscopy (XAS) measurements for the samples were carried out in fluorescence mode using IDEAS beamline at the Canadian Light Source (CLS).

Electrochemical measurements

Preparation of electrode: The catalyst inks were prepared by mixing catalyst (5.0 mg), absolute ethanol (950 μL) and 5 wt% Nafion solution (50 μL) followed sonication for 20 minutes. Subsequently, 5 μL homogeneous ink was dropped onto a glassy carbon electrode with an effective diameter of 3mm and dried under natural conditions.

Electrochemical Measurements: A standard three-electrode system equipped with an electrochemical workstation (CHI 760E) was used to perform CO_2 reduction. The H-type electrolytic cell was separated by an anion exchange membrane with 0.5 M $KHCO_3$ solution saturated by CO_2 (pH=7.2) as electrolyte in each chamber. The counter electrode was a piece of platinum wire. All measured potentials by an Ag/AgCl reference electrode (3.5 M KCl) were converted to the reversible hydrogen electrode (RHE) reference scale using E (vs. RHE) = E (vs. Ag/AgCl) + 0.209 V + 0.0591 V× pH. The electrolyte in the cathodic compartment was bubbled with a steady supply of CO_2 at a rate of 20.00 sccm, under stirring magnetically at a rate of 1300 rpm during electrolysis. For gas product analysis, a gas chromatograph equipped with both the thermal conductivity detection (TCD) and flame ionization detector (FID) was used. Meanwhile, ^{1}H NMR was employed to test for liquid-phase products whose concentration was analyzed on Bruker Avance 400 MHz spectrometer.

The Faradaic efficiency (FE)for a specific product is calculated using the following equation:

$$FE = \frac{z \cdot n \cdot F}{Q}$$

Where z is the number of electrons exchanged, $n$is the number of moles for a specific product, $F$is Faradaic constant, Q is the passed charge.

Computational details

The quantum mechanics (QM) calculations were carried out using the VASP software, version of 5.4.4,[1-3] with the Perdew, Burke, and Ernzerhof (PBE) flavor[4] of density functional theory (DFT). The projector augmented wave (PAW) method[5] was used to account for core-valence interactions. The kinetic energy cutoff for plane wave expansions was set to 400 eV, and reciprocal space was sampled by the Γ-centered Monkhorst-Pack scheme with a grid of 3×3×1. We applied the post-stage DFT-D3 van der Waals correction using with Becke-Johnson damping.[6]

The vacuum layer is at least 15 Å above the surface. The convergence criteria are 1×10^{-7} eV energy differences for solving the electronic wave function. The Methfessel-Paxton smearing of second order with a width of 0.1 eV was applied. All geometries (atomic coordinates) were converged to within 1×10^{-2} eV Å^{-1} for maximal components of forces.

The Gibbs free energies were calculated at 298 K and 1 atm as outlined in:

$$G = H - T\Delta S = E_{DFT} + E_{ZPE} + E_{solv} + \int_0^{298} C_V dT - T\Delta S$$

where E_{DFT} is the DFT-optimized total energy, E_{ZPE} is the zero-point vibrational energy, E_{solv} is the solvation energy. $\int_0^{298} C_V dT$ is the heat capacity, T is the temperature, and ΔS is the entropy Gas-phase molecules such as CO were treated using the ideal gas approximation, whereas adsorbents were treated using a harmonic approximation. The solvation was treated implicitly using the CANDLE method[7] using the JDFTx simulation package. The GBRV[8] ultrasoft pseudopotentials (USPP) were used, with a plane wave cutoff of 544 eV (20 a.u.). All other settings are similar to those in VASP calculations.

The electronic structure of Cu greatly influences on the binding of intermediates to the catalyst surface. We carried out DFT calculations to investigate the effect of Bi alloying in Cu. In our calculations, we constructed three models: Cu_1Bi_1, Cu_3Bi_1 and Cu_7Bi_1.

- The Cu_1Bi_1 is a layer structure.

- Cu_3Bi_1 surface is built from a Cu FCC conventional cell (four atoms in a cell) by replacing one Cu to Bi, leading to a Cu:Bi ratio of 3:1.
- Cu_7Bi_1 is built from a 2×2×2 Cu FCC primitive cell (eight atoms in a cell) by replacing one Cu to Bi, leading to a Cu:Bi ratio of 7:1.

The difference between the Cu_3Bi_1 model and the Cu_7Bi_1 model is that Bi is in every layer of Cu_3Bi_1 while Bi is in every two layers of Cu_7Bi_1. Thus, there is a pure Cu layer in Cu_7Bi_1.

Supporting Figures

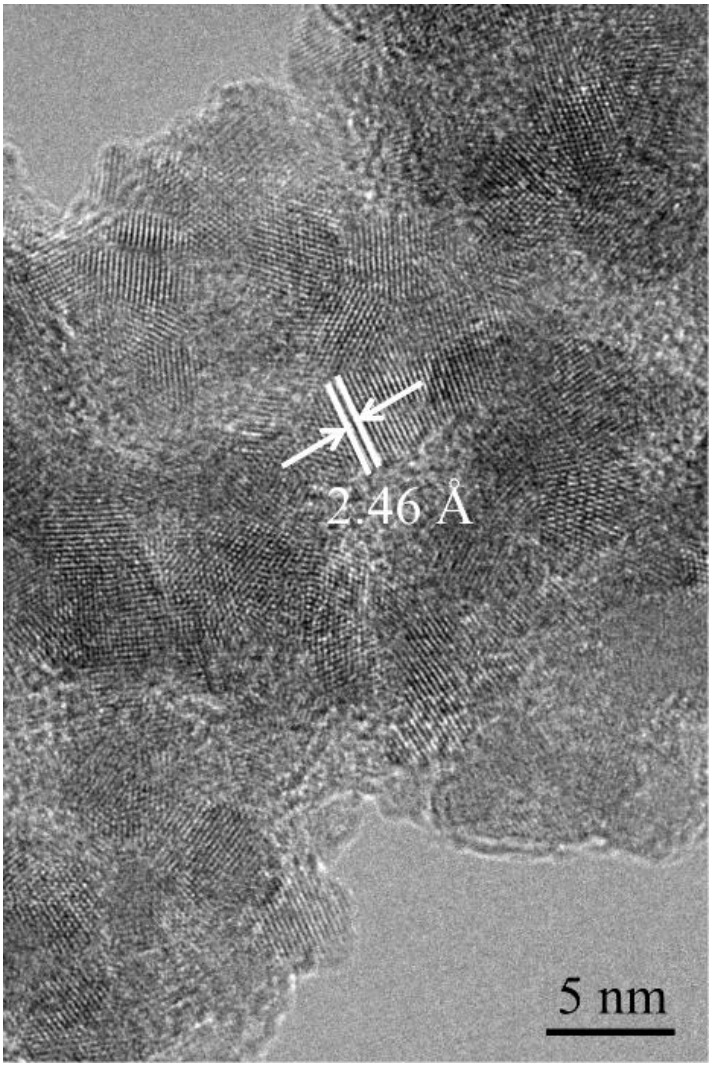

Figure S1. HRTEM image of synthesized Cu NPs. Due to the oxidation, the Cu NPs have the lattice distance of 2.46 Å, corresponding to Cu_2O (111).

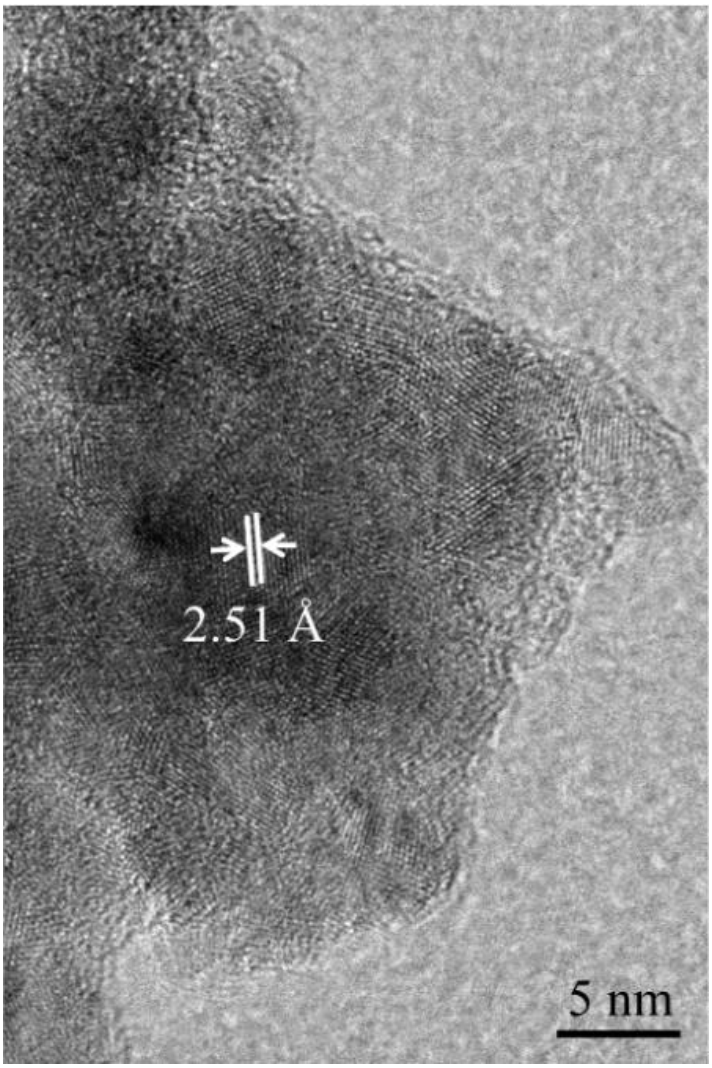

Figure S2. HRTEM image of synthesized Cu_9Bi_1 NPs, which have the lattice distance of 2.51 Å.

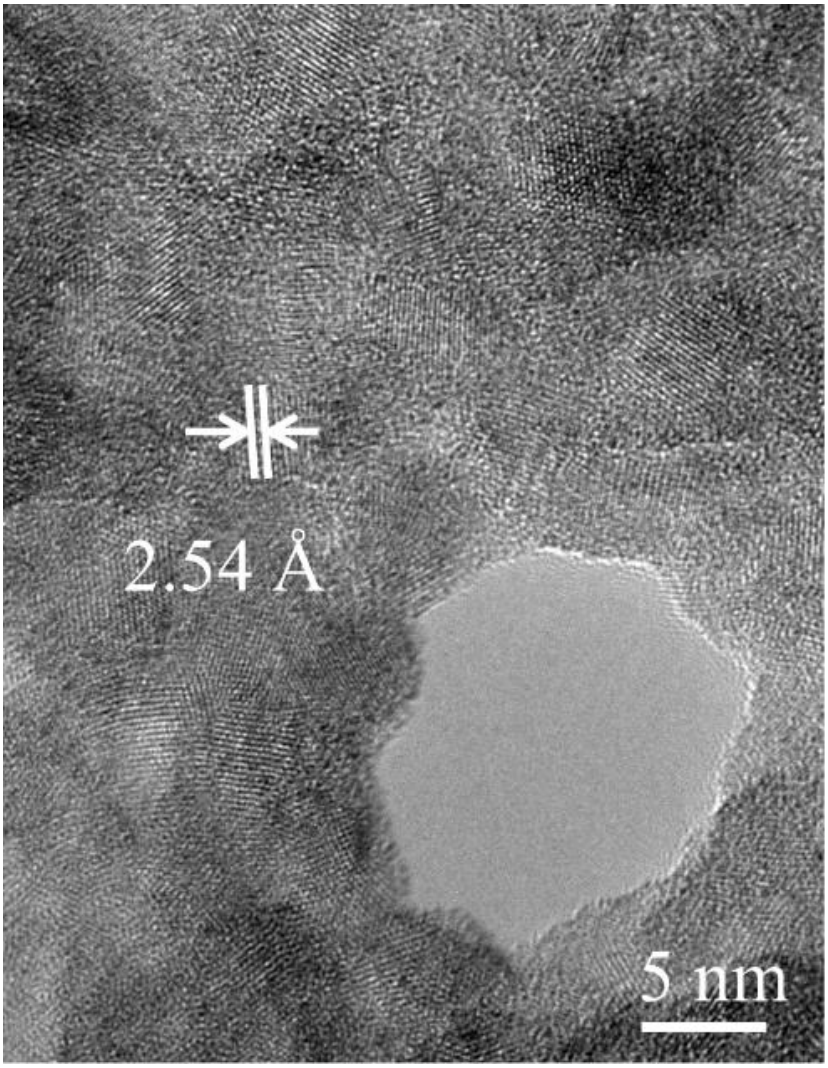

Figure S3. HRTEM image of synthesized Cu_7Bi_1 NPs, which have the lattice distance of 2.54 Å.

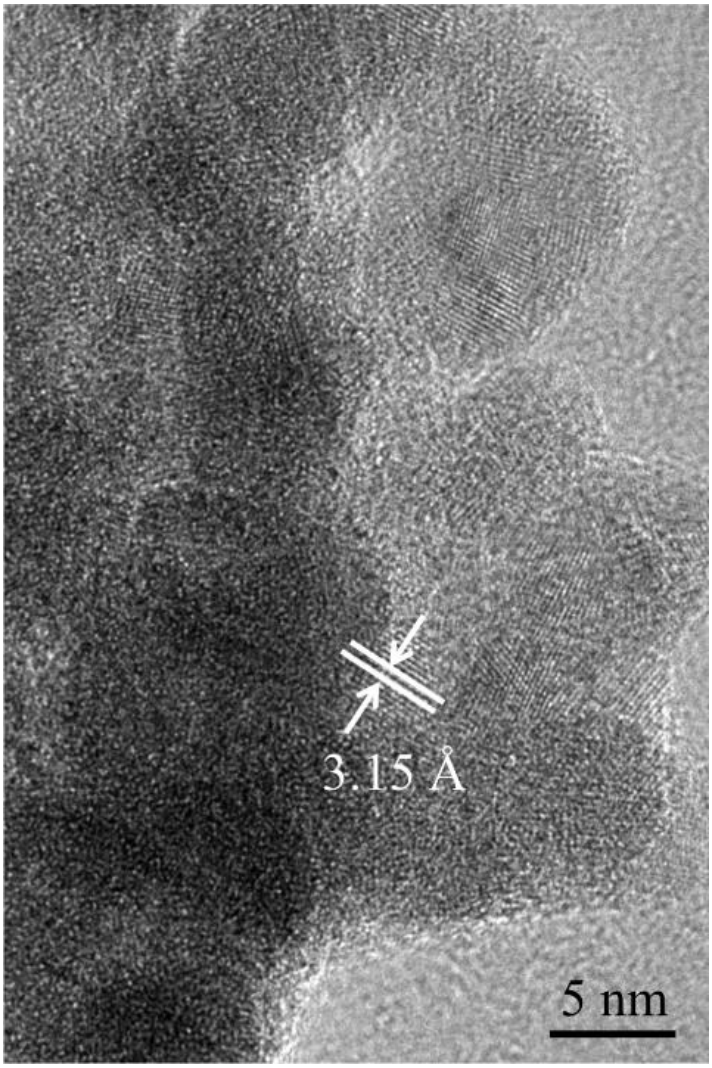

Figure S4. HRTEM image of synthesized Cu_3Bi_1 NPs, which have the lattice distance of 3.15 Å.

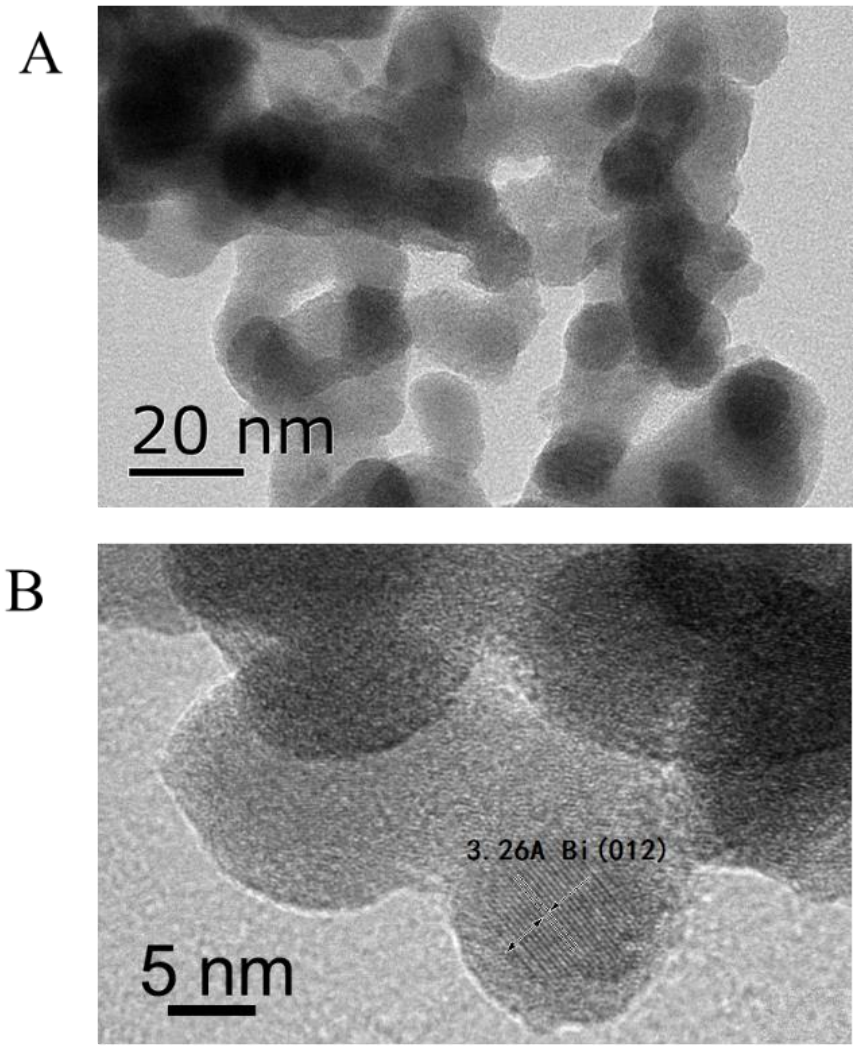

Figure S5. TEM (A) and HRTEM (B) images of synthesized Bi NPs.

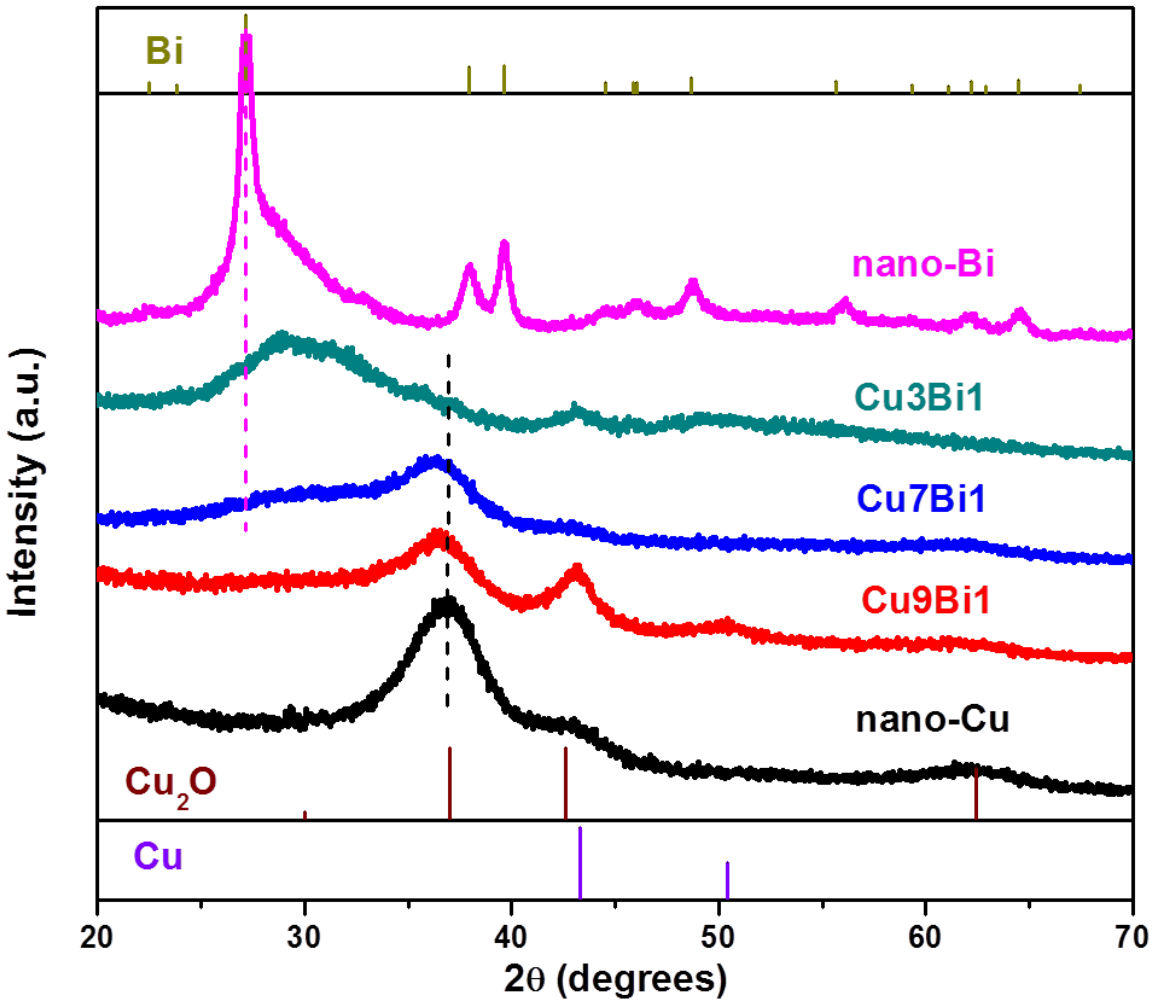

Figure S6. XRD patterns of synthesized Cu NPs, Cu-Bi NPs and Bi NPs.

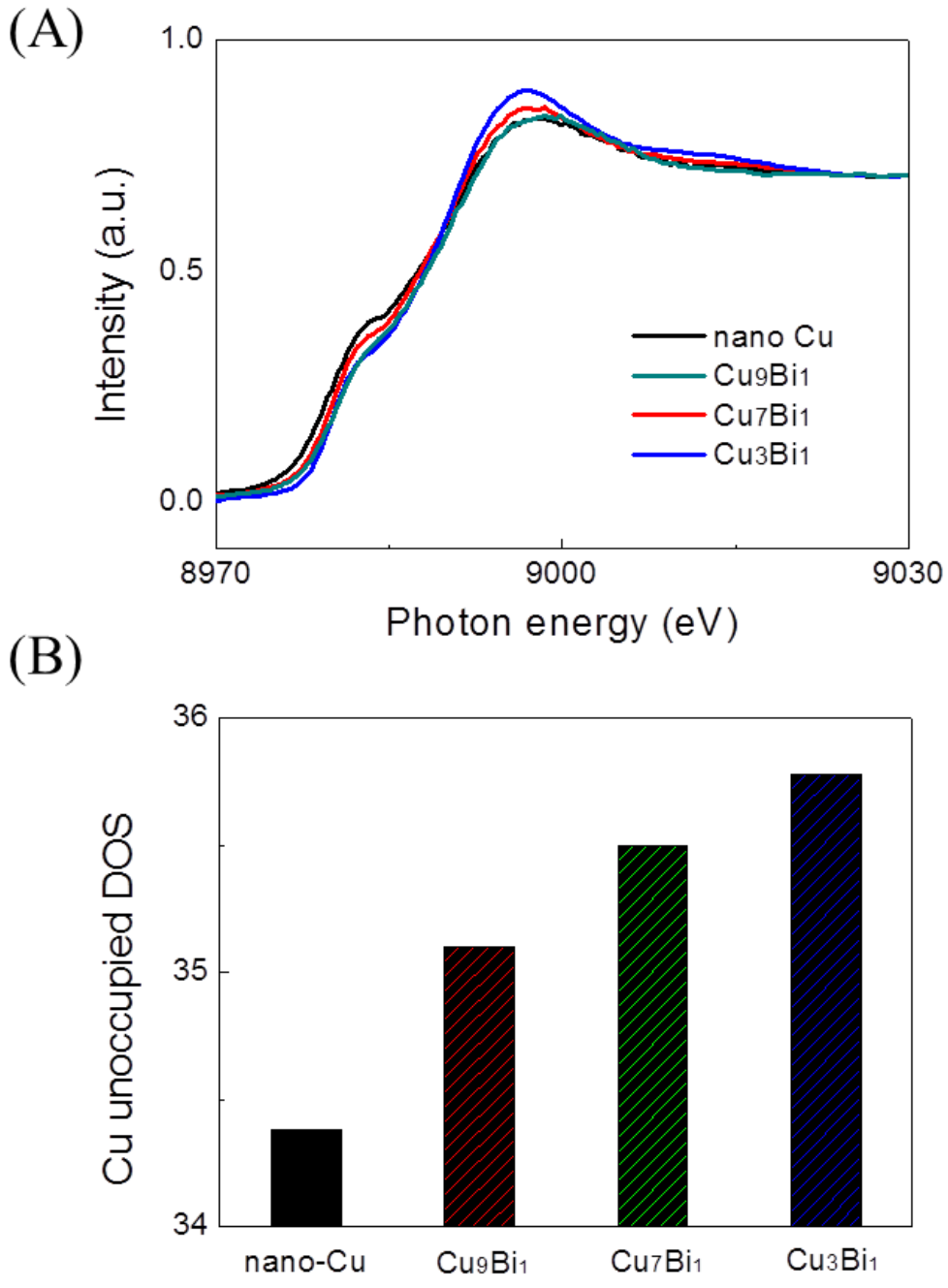

Figure S7. (A) Cu K-edge XANES spectra and (B) summary of the Cu unoccupied DOS of the four Cu-based electrodes.

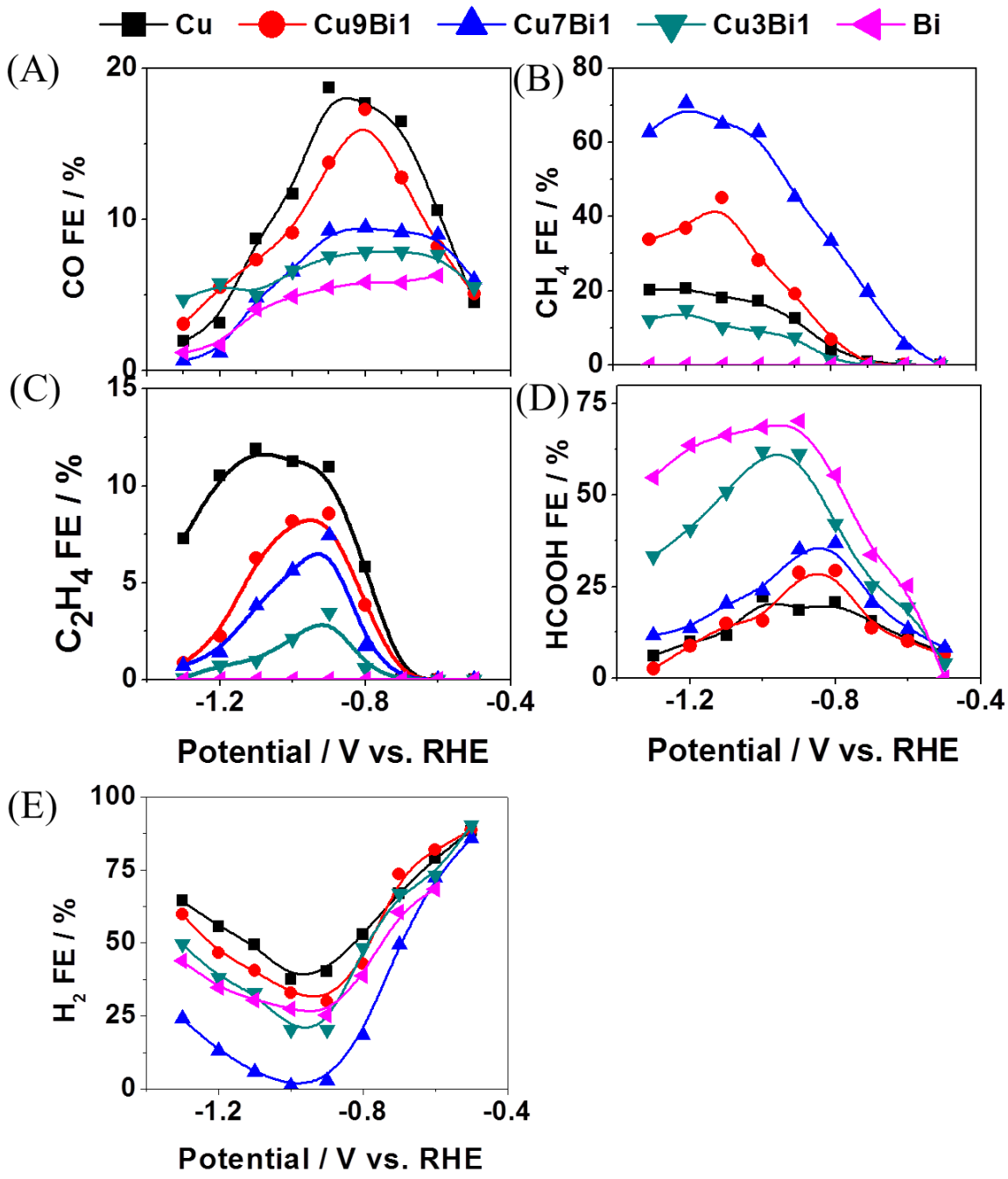

Figure S8. The FE for each product as a function of potential on as-synthesized Cu NPs, Cu_9Bi_1 NPs, Cu_7Bi_1 NPs, Cu_3Bi_1 NPs and Bi NPs during CO_2RR.

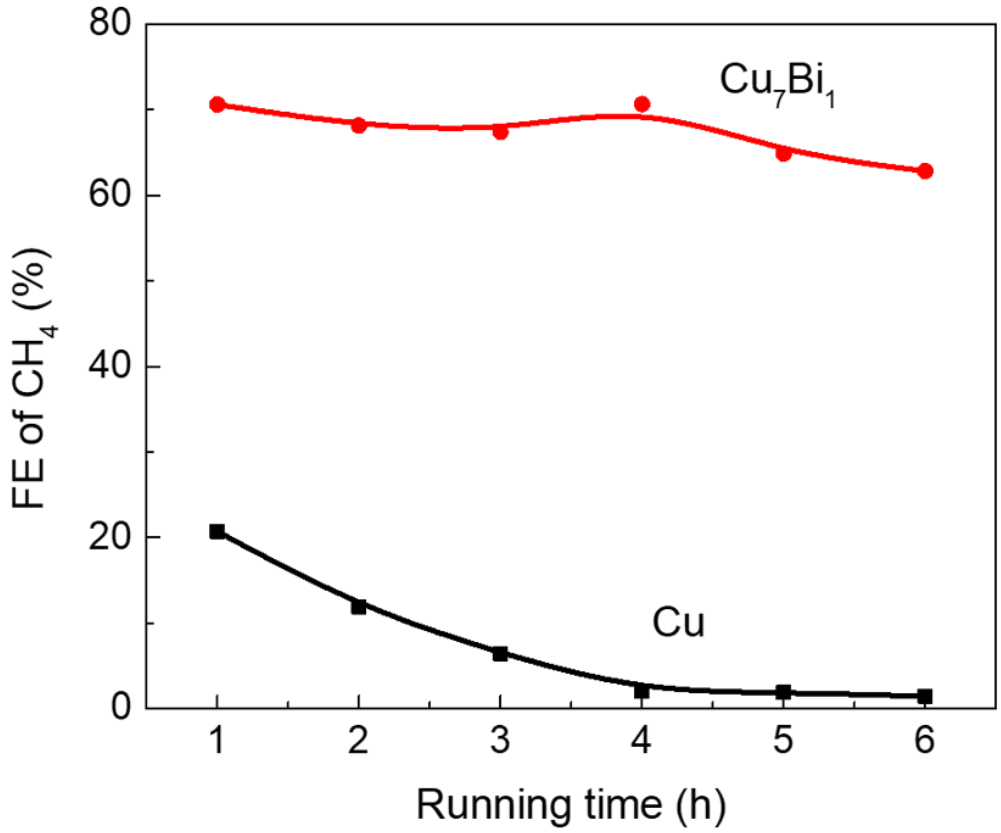

Figure S9. FE for CH_4 at -1.2 V (vs RHE) during 6 h of Cu_7Bi_1 NPs and Cu NPs.

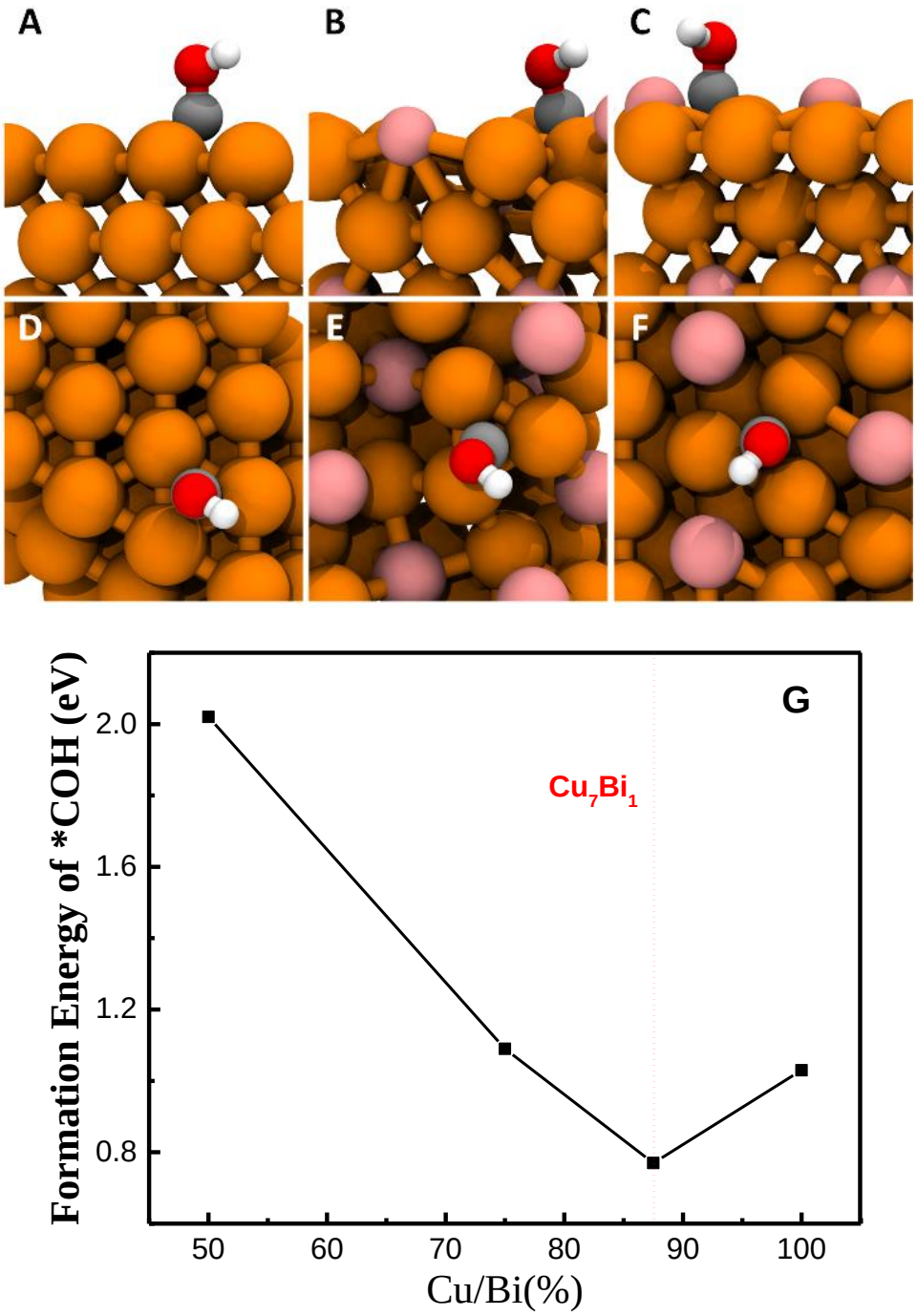

Figure S10. The optimized atomic structures of *COH on Cu NPs from side view (A) and top view (D), on Cu_3Bi_1 NPs from side view (B) and top view (E) and on Cu_7Bi_1 NPs from side view (C) and top view (F), (G) The formation energy of *COH (in eV) of Cu_1Bi_1 NPs, Cu_3Bi_1 NPs, Cu_7Bi_1 NPs and Cu NPs from DFT calculations.

We took three models together with pure Cu NPs to investigate the effect of Bi to CO_2RR ranging from 50% to 100%, which fully covers the experimental concentration. To predict the performance of CO_2RR to CH_4, we took *COH formation energy as the descriptor because in our previous work we found that *COH formation is the potential determining step in CH_4 formation. The optimized atomic structure of *COH on Cu_1Bi_1 NPs, Cu_3Bi_1 NPs, Cu_7Bi_1 NPs and Cu NPs are shown in Figure S10 A to F.

The DFT calculations predict that the formation energies of *COH on Cu_1Bi_1 NPs, Cu_3Bi_1 NPs, Cu_7Bi_1 NPs and Cu NPs are 2.02, 1.09, 0.77 and 1.03 eV, respectively (as shown in Figure 10 G). Thus, we predict the optimum concentration of Cu-Bi towards CH_4 formation is when Bi is less than 23%, which explains the experimental observations that Cu_7Bi_1 NPs exhibits an improved CO_2RR performance to CH_4. Also put in a table of the VASP energies for the minimized structures for each case and the final geometry.

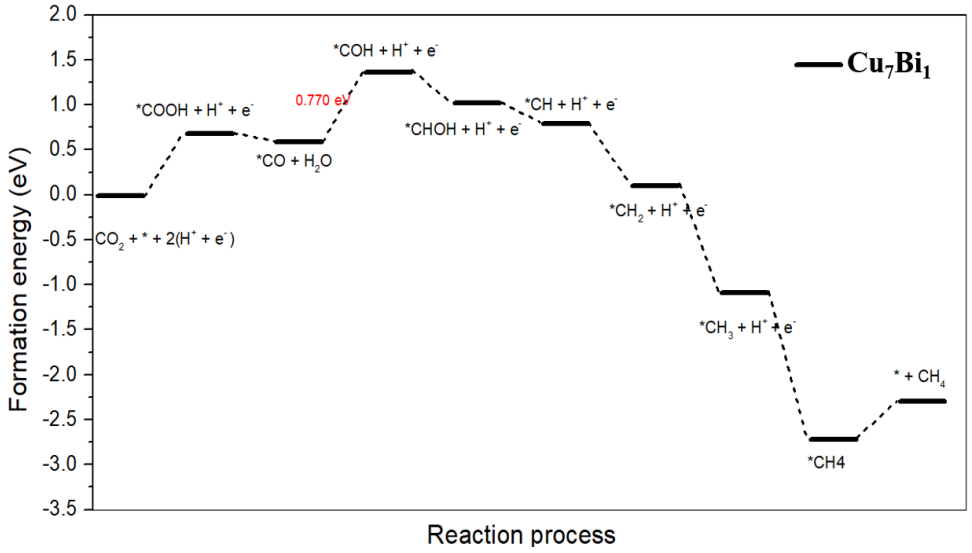

Figure S11. The minimal formation energy pathway of CH_4 formation in Cu_7Bi_1.

From the free energy profile as shown in Figure S11, it is clear that the potential determining step is *COH formation with a potential energy increase of 0.77 eV, indicating at least -0.77 V applied potential to drive the reactions. This 0.77 V redox potential is 0.14 eV lower than that of Cu(111). Therefore, we concluded that the CH_4 formation is enhanced with introduction of Bi.

References

(1) Kresse, G.; Hafner, J. Ab. initio molecular dynamics for liquid metals. *Phys. Rev. B* **1993,** *47*, 558-561.

(2) Kresse, G.; Furthmuller, J. Efficiency of ab-initio total energy calculations for metals and semiconductors using a plane-wave basis set. *Comp. Mater. Sci.* **1996,** *6*, 15-50.

(3) Kresse, G.; Furthmuller, J. Efficient iterative schemes for ab initio total-energy calculations using a plane-wave basis set. *Phys. Rev. B* **1996,** *54*, 11169-11186.

(4) Perdew, J. P.; Chevary, J. A.; Vosko, S. H.; Jackson, K. A.; Pederson, M. R.; Singh, D. J.; Fiolhais, C. Atoms, molecules, solids, and surfaces: Applications of the generalized gradient approximation for exchange and correlation. *Phys. Rev. B* **1992,** *46*, 6671-6687.

(5) Fishman, M.; Zhuang, H. L. L.; Mathew, K.; Dirschka, W.; Hennig, R. G. Accuracy of exchange-correlation functionals and effect of solvation on the surface energy of copper. *Phys. Rev. B* **2013,** *87*, 245402.

(6) Grimme, S.; Antony, J.; Ehrlich, S.; Krieg, H. A consistent and accurate ab initio parametrization of density functional dispersion correction (DFT-D) for the 94 elements H-Pu. *J. Chem. Phys.* **2010,** *132*, 154104.

(7) Sundararaman, R.; Goddard, W. A. The charge-asymmetric nonlocally determined local-electric (CANDLE) solvation model. *J. Chem. Phys.* **2015,** *142*, 064107.

(8) Garrity, K. F.; Bennett, J. W.; Rabe, K. M.; Vanderbilt, D. Pseudopotentials for high-throughput DFT calculations. *Comp. Mater. Sci.* **2014,** *81*, 446-452.